Time-dependent density functional theory studies of the electronic absorption spectra of *N,N′*-disubstituted 2,3-dialkynyl-1,4-diazabuta-1,3-dienes

Linnea E. Forslund, Rüdiger Faust and Nikolas Kaltsoyannis †

Department of Chemistry, University College London, 20 Gordon Street, London, UK WC1H 0AJ. E-mail: n.kaltsoyannis@ucl.ac.uk

Received (in Cambridge, UK) 29th October 2001, Accepted 3rd December 2001
First published as an Advance Article on the web 17th January 2002

The electronic structures and transition energies of the title compounds are studied computationally using time-dependent density functional theory. A computationally tractable model chemistry is established, involving the local density approximation in conjunction with double-zeta plus polarisation basis sets. Solvent effects are included *via* the conductor-like screening model. Good agreement is found between the computationally determined geometric structures of several of the title systems and those found experimentally for related molecules. The electronic transition energies of all of the systems studied are found to be strongly influenced by the dihedral angle between the aryl rings and the backbone of the diazabutadiene unit. Satisfactory interpretation (at the molecular orbital level) of experimentally determined electronic absorption spectra is obtained using computational model compounds in which the acetylenic $^{i}Pr_3Si$ substituents are replaced by hydrogen atoms. Inclusion of the $^{i}Pr_3Si$ units in the calculations leads to a simulated spectrum which is more complicated than that of the H-substituted system. Comparison with experiment does not conclusively establish if the $^{i}Pr_3Si$ units are required in the computational model. The implications for future simulations of the electronic absorption spectra of diazabutadiene complexes of transition metals are discussed.

Introduction

Photodynamic Therapy (PDT)[1–3] is a relatively new treatment for a range of cancers, and as such represents a therapeutic method which is complementary to standard chemotherapeutic or surgical approaches. At the core of PDT are photosensitising dyes with strong absorptions in the far red end of the visible or in the near infrared (NIR) region of the spectrum.[4] Appropriately substituted nitrogen-containing macrocycles based on porphyrin[5] or phthalocyanine[6,7] backbones have been investigated with a view to their PDT applicability. We have focused on the possibility that acetylenic NIR dyes may well find application in PDT[8] and, as part of these studies, have been interested in exploring the electronic structures and properties of *N,N′*-disubstituted 2,3-dialkynyl-1,4-diazabuta-1,3-dienes (DADs)[9] and their complexes with group 10 transition metals.[10] We have noted that the optical properties of palladium complexes of DAD molecules with aryl substituents on the nitrogen atoms show a striking dependence upon the substitution pattern of the aryl rings. Specifically, the presence of an electron-donating dimethylamino substituent on the iminoaryl group results in sizeable NIR absorptions.[11] However, the electronic origin of these absorptions is unclear, although it does appear that both alkynyl and *N*-aminoarylimino moieties are required to induce sizeable low-energy transitions.

In order to gain further insight into the electronic absorption spectra of DADs and their transition metal complexes, we have turned to computational techniques in the form of time-dependent density functional theory (TD-DFT). Although TD-DFT has been in place for some time,[12] it is only recently that computational implementations[13] have allowed its application to molecules (see, for example, references 14–16), and we were very keen to establish the efficacy of the technique for the prediction of the electronic absorption spectra of large organic and organometallic systems. The eventual aim of this project is to be able to design molecules with the correct photophysical properties for PDT, specifically molecules with strong NIR absorptions.

In this contribution we report the results of the first part of the project, *i.e.* computational studies of the electronic absorption spectra of several alkynyl-substituted DAD molecules. This work sought initially to establish the best model chemistry (*i.e.* set of computational parameters) for this type of calculation. Subsequently we have compared calculated electronic absorption spectra with those obtained experimentally for several of the title systems,[9] and thus have gained a measure of the accuracy of the computational technique. Finally, we have evaluated the extent to which it is possible to simplify the chemical model used in our calculations while retaining reasonable agreement between theory and experiment. Specifically, we have sought to establish if the computationally demanding acetylenic $^{i}Pr_3Si$ substituents, present in the experimentally studied systems, can be justifiably replaced by H atoms.

Computational details

All calculations were performed on Compaq ES40 and Digital Personal Workstation 433au computers using the Amsterdam Density Functional program suite, versions 2.3, 1999 and 2000.[17–21] Uncontracted, valence-only Slater-type orbital basis sets were employed, the quality of which varied as is discussed in the main text, but which were predominantly double-zeta with a single polarisation function (ADF Type III). The frozen core approximation was employed; carbon (1s), nitrogen (1s) and silicon (2p). The local density parameterisation of Vosko, Wilk and Nusair[22] was employed, together with a range of gradient corrections as discussed in the main text. The majority of the calculations, however, were performed using the local

† http://www.chem.ucl.ac.uk/people/nkalt/index.html

 DOI: 10.1039/b109863m

density approximation. Excitation energies were computed using the time-dependent methods implemented in ADF.[13] Solvent effects were included using the COSMO of solvation.[23] Molecular orbital plots were generated using the program MOLDEN, written by G. Schaftenaar of the CAOS/CAMM Centre, Nijmegen, The Netherlands. The same MOLDEN 'space' value—0.05—has been used for all plots. The ADF binary output files (TAPE21) were converted to MOLDEN format using the program ADFrom99 written by F. Mariotti of the University of Florence.[24]

Results and discussion

Several different DAD molecules have been chosen as computational targets for the present study. Scheme 1 indicates

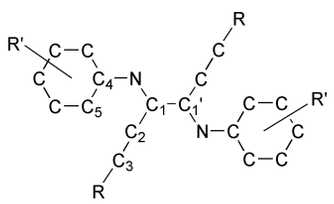

Compound	R	R'
1	H	H
2	$^{i}Pr_3Si$	H
3	H	4-Me_2N
4	C_6H_5	H
5	$^{i}Pr_3Si$	3,5-Me_2
6	$^{i}Pr_3Si$	4-Me_2N

Scheme 1

these, together with experimentally studied systems with which extensive comparisons are drawn. The acetylenic and aryl substituents are indicated, as is the atom numbering system adopted in this paper.

A Choosing a model chemistry

The molecules studied in the present work are large by the standards of quantum chemistry. It was therefore important that we established a model chemistry (*i.e.* a set of computational parameters) which produced good results while retaining computational feasibility. This is particularly important as this study is the first in which we have used TD-DFT to calculate electronic transition energies (although we do have previous experience with the fractional occupancy method of Slater[25,26]) and, as described below, the collective experience of the application of TD-DFT methods to molecular systems is comparatively limited. To this end we chose planar **1** in the (*E*-s-*trans*-*E*) orientation as a target system on which to evaluate the effects of altering the computational parameters. The (*E*-s-*trans*-*E*) orientation was chosen as this is the arrangement found crystallographically for **4** and **5**.[9] The imposition of planarity does not agree with experiment (the aryl rings are found to be significantly rotated out of the plane of the DAD backbone—see section A5 for a comparison of experimental and calculated geometries), but was adopted to ensure the highest possible symmetry (C_{2h}), and hence most efficient computation, in these trial calculations.

A1 How good are TD-DFT methods? Before describing the results of our search for a model chemistry, it is worth taking a moment to consider the current state of TD-DFT methods. The application of the approach to molecular systems is comparatively new, although the field is expanding rapidly. We cannot, of course, provide a comprehensive review of the field in this paper; instead we briefly discuss three recent and representative studies of the application of TD-DFT to inorganic and organic molecules. van Gisbergen *et al.* have calculated the electronic transition energies in $[MnO_4]^-$, $Ni(CO)_4$ and $Mn_2(CO)_{10}$ using both TD-DFT and *ab initio* approaches.[14] They concluded that the performance of TD-DFT is at least as good as that of *ab initio* methods for small molecules, and certainly superior for large systems (for which good-quality *ab initio* calculations remain unfeasible). They also found that all of the theoretical methods they tried, including TD-DFT, occasionally exhibited deviations of up to 1 eV when compared with experimental transition energies. Furthermore, they noted that the approximate nature of the exchange-correlation functional in TD-DFT calculations leads to sources of error which are difficult to quantify.

Matsuzawa *et al.* have used TD-DFT to calculate the transition energies and oscillator strengths of four organic molecules: formaldehyde, benzene, ethylene and methane.[15] In agreement with van Gisbergen *et al.*, they found that TD-DFT is generally superior to *ab initio* approaches, producing at least semi-quantitative agreement between experiment and theory. They concluded that the local density approximation underestimates transition energies by up to 1.3 eV, and that the inclusion of gradient corrections improves agreement with experiment in all cases except for benzene, where no improvement was found. They also noted that the basis set dependence of the transition energies was not as pronounced as that of the exchange-correlation functional.

Gobbi *et al.* have recently reported the results of a combined experimental and TD-DFT study of *N,N*-dialkylaniline-substituted tetraethynylethenes, systems not unrelated to our target molecules.[16] Their calculations showed remarkable agreement with experiment, superior to that reported by van Gisbergen *et al.* and Matsuzawa *et al.*, with typical discrepancies of 10 nm or less (< 0.1 eV). It would therefore appear that the performance of the TD-DFT approach is quite system-dependent, as is the effect of altering the computational parameters. It was therefore important that we established a good model chemistry for our target molecules, and it is to this that we now turn.

A2 Basis set. In order to probe the effects of basis set alteration we conducted a series of calculations on planar **1** in which the basis set was varied from single zeta (sz, ADF Type I) to double zeta plus a single polarisation function (dz1p, ADF Type III) and finally triple zeta plus two polarisation functions (tz2p, ADF Type V). Each calculation included the effects of dichloromethane solvent (ε = 8.9) *via* the COSMO using the Klamt surface,[27] and the LDA was used. In each case the geometry of the molecule was optimised and the singlet–singlet electronic transition energies and oscillator strengths calculated. The results are presented in Table 1 (only those transitions with oscillator strengths above 0.1 are included).

The transitions are separated into two groups in Table 1. The four lowest energy transitions (3.48–6.63 eV for sz) retain their principal MO character as the basis set is altered (*N.B.* we do not discuss the orbital character of the transitions at this stage, but do so extensively below, see sections B2 and B3). The remainder of the transitions vary in character as the basis set is altered, and hence are listed in separate rows. In order to ensure a like-for-like comparison, we confine our discussion to the four lowest energy transitions. All four transitions display a significant shift to lower energy as the basis set is altered from sz to dz1p. The intensities do not show quite the same basis set dependence, although it is noticeable that the relative intensities of the 5.56 and 6.63 eV transitions are reversed on moving to dz1p. Moving to from dz1p to tz2p produces much smaller changes in energy than from sz to dz1p, and the oscillator strengths are similar. From this we conclude that the dz1p basis set should be adequate for our purposes; the additional expense of tz2p is not warranted.

Table 1 Calculated transition energies (eV), wavelengths (nm) and oscillator strengths for planar **1** with different basis sets

sz			dz1p			tz2p		
Energy	Wavelength	Oscillator strength	Energy	Wavelength	Oscillator strength	Energy	Wavelength	Oscillator strength
3.48	356	0.84	3.07	403	0.91	3.03	409	0.91
5.16	240	0.16	4.57	271	0.17	4.52	274	0.16
5.56	223	0.18	5.27	235	0.12	5.23	237	0.15
6.63	187	0.13	6.35	195	0.20	6.16	201	0.18
						6.45	192	0.11
						6.73	184	0.50
			6.81	182	0.31			
			6.85	181	0.23			
						6.85	181	0.19
						6.96	178	0.38
			7.00	177	0.27			
			7.16	173	0.33			
7.94	156	0.40						
8.37	148	0.16						
8.49	146	0.49						

Table 2 Calculated transition energies (eV), wavelengths (nm) and oscillator strengths for planar **1** with different exchange-correlation functionals

LDA (VWN)			PW91			BLYP			BP86		
Energy	Wavelength	Oscillator strength	Energy	Wavelength	Oscillator strength	Energy	Wavelength	Oscillator strength	Energy	Wavelength	Oscillator strength
3.07	403	0.91	3.07	404	0.89	3.11	399	0.86	3.06	405	0.88
4.57	271	0.17	4.54	273	0.20	4.56	272	0.21	4.53	273	0.20
5.27	235	0.12	5.23	237	0.13	5.26	235	0.14	5.21	238	0.13
6.35	195	0.20	6.45	192	0.21	6.44	192	0.19	6.45	192	0.22

A3 Exchange-correlation functional. The introduction of gradient corrections into density functional calculations carries a significant computational overhead (typically a factor of two in ADF calculations). For many purposes, however, it is necessary to include such corrections in order to obtain good results, and we therefore evaluated several of the most widely used extensions to the LDA. Each calculation included the effects of dichloromethane solvent *via* the COSMO using the Klamt surface, and the dz1p basis set was used. As in section A2, the geometry of the molecule was optimised in each case, and the singlet–singlet electronic transition energies and oscillator strengths calculated. The results for the four lowest energy singlet–singlet transitions are given in Table 2, from which it may be seen that the inclusion of gradient corrections does not significantly alter either the energies or oscillator strengths. ‡ We therefore conclude that the LDA will suffice for the present study.

It should be noted that, as with the basis set calculations, the MO character of the transitions below 200 nm varied considerably as the exchange-correlation functional was altered, while that of the lower energy transitions remained quite constant (making it much easier to evaluate the effect of changing the functional on a particular transition). It would appear, therefore, that the calculation of high energy transitions in our systems is much more sensitive to the choice of computational parameters than is that of the longer wavelength transitions. Fortunately, we are interested primarily in the lowest energy transitions in this work and its extension to transition metal complexes of DADs.

A4 Solvent surface. The experimental UV/vis spectral data which we wish to reproduce and rationalise have, of course, been obtained in solution. We have therefore included the effect of the solvent in all of our electronic transition energy calculations through the COSMO approach.§ Four methods for modelling the COSMO solvent surface are implemented within ADF. We have studied the effect of each on the electronic transitions of planar **1**, using dichloromethane as a solvent, the LDA and the dz1p basis set. As before, in each case the geometry of the molecule was optimised, and the singlet–singlet electronic transition energies and oscillator strengths calculated. We found that the choice of surface made very little difference to the energies and oscillator strengths of the lower energy transitions. However, subsequent experience revealed that the Klamt surface was the most stable computationally, and hence has been employed throughout the present work.

A5 Comparison of experimental and calculated geometries. From the test calculations described above we conclude that a good model chemistry which is computationally tractable uses the dz1p basis set in conjunction with the VWN parameterisation of the LDA and, for the inclusion of solvent effects, the Klamt surface. Before embarking on our study proper, we decided to compare the calculated (gas-phase) geometries of some of our target systems with those determined experimentally on related compounds. These geometry optimisations use the LDA–dz1p combination and relax the symmetry to C_2, *i.e.* the planarity constraint is removed. Selected metric parameters from our calculations and previous X-ray crystallographic studies are collected in Table 3.

There is generally excellent agreement between theory and experiment, with most bond lengths calculated to within 0.03 Å of the experimental value. Within the DAD unit itself, the C_1–N

‡ This is in contrast to the majority of the data reported by Matsuzawa *et al.*, but in agreement with their findings for benzene.[15]

§ We have also performed excitation energy calculations on gas-phase **1**, *i.e.* calculations in which the effects of solvent have not been included. The results suggest that the effect on both transition energies and oscillator strengths of including the solvent *via* the COSMO approach is comparatively limited (*e.g.* wavelength changes of a few nm) but we have nevertheless retained solvent effects in our calculations as they are not a major computational expense and because we wish, in a subsequent study, to examine the effects of changing the solvent on both experimental and calculated spectra.

Table 3 Selected computational and experimental metric parameters for DAD molecules. Bond lengths in Å, bond/dihedral angles in °. See Scheme 1 for atom numbers

Compound	C_1–C_1'	C_1–N	C_1–C_2	C_2–C_3	N–C_4	C_3–Si	N–C_1–C_1'	N–C_1–C_2	C_1–N–C_4–C_5
1 (calc)	1.474	1.280	1.412	1.207	1.380	—	117.3	126.2	53.0
2 (calc)	1.468	1.286	1.406	1.217	1.384	1.815	117.8	125.0	52.0
3 (calc)	1.472	1.289	1.418	1.210	1.364	—	116.5	129.4	0.0
4 (exp)[a]	1.491(2)	1.282(2)	1.441(2)	1.185(2)	1.427(3)	—	117.8	125.2	55.1
5 (exp)[a]	1.491(2)	1.272(2)	1.442(3)	1.196(3)	1.427(3)	1.847(2)	118.3	124.0	80.9

[a] Data from reference 9.

distances are reproduced essentially exactly, while the central C_1–C_1' distance is slightly shorter than found experimentally (the comparatively long central C–C bond is a feature of these DAD systems[9]). Compared with experiment, the calculated C_1–C_2 distance is slightly short and the acetylenic C_2–C_3 distance slightly long, but the differences are small. The largest discrepancy (0.05 Å) is found for N–C_4 but, given the agreement in the rest of the data, we feel that this can be tolerated.

There is also a close match between the experimental and calculated angles. In particular, the experimental finding that the aryl rings are significantly rotated out of the DAD plane is pleasingly reproduced by our calculations. As we shall see, the rotation of the aryl rings about the N–C_4 bond has a pronounced effect on the calculated absorption spectra, and hence it is important that our model chemistry reproduces this experimental structural feature. The exception is **3**, for which a coplanar geometry is favoured computationally. However, further studies revealed that the potential surface for rotation of the aryl rings about the N–C_4 bond in **3** is very flat, with structures up to *c*. 35° being almost isoenergetic. We return to this below.

B Electronic transitions and UV/Vis spectra

B1 Molecular geometry in solution. As discussed in section A, the (*E*-s-*trans*-*E*) orientation is found in the X-ray structures of **4** and **5**.[9] In order to establish which conformation—s-*cis* or s-*trans*—is the more likely to exist in solution, we calculated the barrier to rotation about the C_1–C_1' bond in planar **1**, including the effects of dichloromethane solvent. The s-*trans* form was found to be 20 kJ mol^{-1} more stable than the s-*cis*, with a 32 kJ mol^{-1} barrier to s-*trans* ⟶ s-*cis* conversion. From this we conclude that the s-*trans* conformation will dominate in solution, and have assumed this conformation in all of our electronic transition calculations.

Initial studies of the energies, intensities and MO characters of the longest wavelength transitions in **1** revealed that they are very sensitive to the C_1–N–C_4–C_5 dihedral angle. For example, the wavelength of the lowest energy transition increases from 455 to 478 nm as the C_1–N–C_4–C_5 angle changes from 10° to 30°, and the oscillator strength more than doubles. It is therefore clear that the C_1–N–C_4–C_5 dihedral angle must be carefully modelled when seeking agreement between experimental and theoretical spectra. We therefore decided to calculate the energy of **1** as both of the aryl rings are rotated simultaneously from C_1–N–C_4–C_5 = 0° to 90°. C_2 symmetry was retained throughout these calculations, and all of the other geometric parameters were optimised at each fixed C_1–N–C_4–C_5 angle. The results are shown in Fig. 1, from which it is clear that the potential surface for rotation about N–C_4 is quite shallow (*c*. 15 kJ mol^{-1} between 0° and just over 50°), particularly around the minimum energy conformation. It is therefore highly likely that there will be molecules with different aryl ring dihedral angles contributing to the experimentally observed UV/Vis spectra.

B2 Comparison of the calculated electronic absorption spectrum of 1 with the experimentally determined spectrum of 2. Given the sensitivity of the calculated transitions to the aryl ring dihedral angle, we decided to calculate the electronic transitions of **1** with C_1–N–C_4–C_5 angles around the minimum energy value, and then to weight the calculated energies and intensities by Boltzmann factors derived from the relative energies of the geometric structures. We found that structures with aryl ring dihedral angles of *c.* ±5° from the minimum energy structure (53°) contributed significantly when weighted by their Boltzmann factor. As both the energies and intensities vary with dihedral angle, the Boltzmann weighting produces a series of different energies and corresponding intensities. We have used the Boltzmann-weighted transition energies and intensities to produce the simulated absorption spectrum shown in Fig. 2, which also shows the experimentally determined UV/Vis spectrum of **2**. Both experiment and theory have used dichloromethane as a solvent. The experimental spectrum shows two bands at wavelengths longer than *c.* 220 nm, with maxima at 265 and 376 nm. Encouragingly, the calculated spectrum also shows two low energy peaks, centred at 334 and 505 nm (note that the calculated and measured intensities of the longest wavelength peak have arbitrarily been set equal to one another in constructing Fig. 2). We therefore suggest that

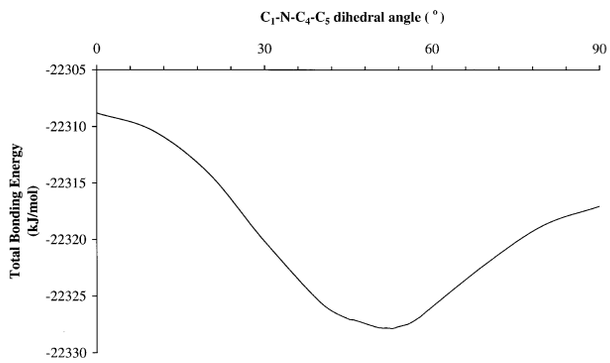

Fig. 1 The total molecular bonding energy of **1** as a function of the C_1–N–C_4–C_5 dihedral angle.

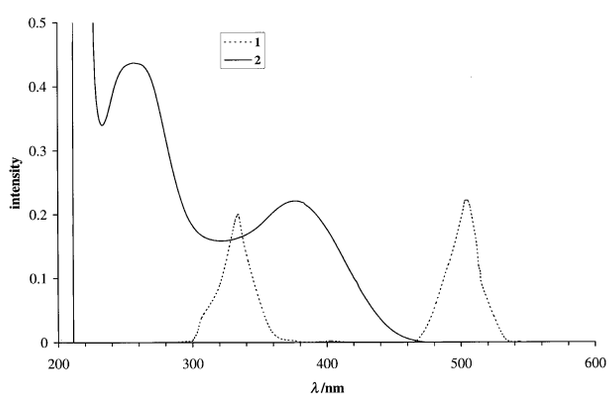

Fig. 2 The experimental UV/Vis absorption spectrum of **2** (solid line) and the simulated spectrum of **1** (dashed line). The intensity of the longest wavelength peak in the simulated spectrum of **1** has been set equal to that in **2**.

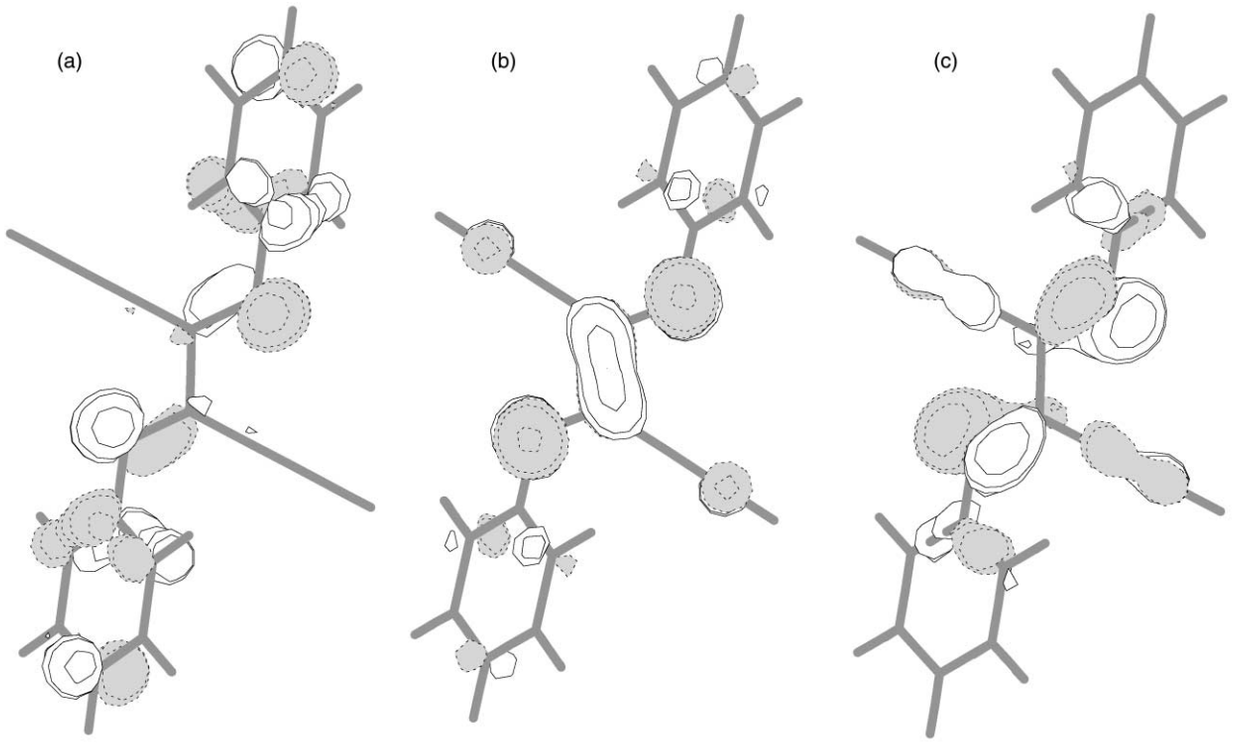

Fig. 3 Three dimensional representations of (a) the 23b HOMO, (b) the 25a LUMO and (c) the 21b HOMO-5 of **1**.

the calculated peak at 505 nm equates with the experimental one at 376 nm, with a similar match between the 334 and 265 nm peaks. The calculated and experimental spectra could be made to match very closely by shifting the calculated spectrum to shorter wavelengths by *c.* 100 nm.

In agreement with Matsuzawa *et al.*,[15] we find that the LDA TD-DFT approach underestimates experimental transition energies. The magnitude of the underestimate, *c.* 0.85 eV for the lower energy transition and *c.* 0.97 eV for the higher energy transition, is comparable with the data reported by these workers, although not as good as that found by Gobbi *et al.*[16] Although the quantitative agreement between theory and experiment for the energies of the two long wavelength peaks is not perfect, we nevertheless feel that we can attempt an assignment of the experimental spectrum on the basis of our calculations. The longest wavelength band, calculated at 505 nm, is found to be due to a $^1B \longleftarrow {}^1A$ transition made up almost entirely (97%) of promotion of an electron from the 23b HOMO to the 25a LUMO.¶ Three dimensional representations of these orbitals are shown in Fig. 3(a) and (b) respectively, from which it may be seen that the HOMO is a mixture of the e_1 level of the aryl rings (*i.e.* the C $2p_\pi$ orbital with one vertical node) and DAD N, while the LUMO is predominantly of DAD π_3 character (*i.e.* the N–C–C–N p_π orbital with two nodes perpendicular to the plane of the backbone). The LUMO is also the destination level in the main transition giving rise to the shorter wavelength band (334 nm). The starting orbital (the 21b HOMO-5), however, is in this case a mixture of DAD π_2 and the acetylenic π bonding level, and is shown in Fig. 3(c).

The experimental and calculated wavelengths are collected in Table 4,‖ together with the principal character of the initial and final MOs of the main electron promotions giving rise to the calculated absorption energies. Examination of this Table reveals that the calculations on **1** find a transition (at 330 nm) which is almost isoenergetic with the 334 nm transition discussed above. The intensity of this transition is calculated to be significantly less than that at 334 nm, but it may well contribute to the higher energy peak in the experimental spectrum of **2**. In orbital terms this absorption is primarily due to promotion of an electron from the 24a HOMO-1 to the 24b LUMO+1, the characters of which are given in Table 4.

Fig. 2 shows that the calculated band centred at 334 nm in **1** has a high energy shoulder. This is calculated to lie at 308 nm, and results almost entirely from promotion of an electron from the 20b HOMO-7, which is of acetylene π bonding character, to the 25a LUMO.

In the experimental spectrum of **2** (Fig. 2) the peak at 265 nm has a higher intensity than that of the 376 nm peak. This is not found in our calculations; the two transitions are predicted to have almost equal oscillator strengths. It is perhaps the case that the intensity of the 265 nm peak in **2** is boosted by its energetic proximity to the very intense band at just above 200 nm. ** Alternatively it may simply be that the calculation of absorption intensities is not in quantitative agreement with experiment, as indeed we have found for transition energies.

B3 Comparison of the calculated electronic absorption spectrum of 3 with the experimentally determined spectrum of 6. It has been found that introducing the strongly electron donating Me_2N group at the *para* position of the aryl rings results in a large bathochromic shift of the longest wavelength transition in the UV/Vis spectrum.[9] This is illustrated by the data for compound **6**, given in Table 4. The longest wavelength peak is shifted bathochromically by 110 nm in comparison with **2**. The shorter wavelength peak of **2** (at 265 nm) is unmoved in **6**, although the peak does display a long wavelength shoulder in **6**, at 322 nm, which is not visible in **2**. It is also noticeable that, by contrast to **2**, the 486 nm peak in the spectrum of **6** is significantly more intense than that at 264 nm.

In order to gain insight into these observations we have calculated the electronic transitions of **3**, a model for **6**. As with **1**, we have assumed that the (*E*-s-*trans*-*E*) orientation prevails in solution. By contrast to **1**, and as noted in section A5, we found

¶ Note that all of the calculated transitions are of $^1B \longleftarrow {}^1A$ symmetry.
‖ Note that, in this Table, the calculated wavelengths (and energies) are the values when the corresponding transition is at its most intense (including the Boltzmann weighting factor).

** This band is due to absorption by atmospheric O_2,[28] and hence is not reproduced by our calculations.

Table 4 Experimental and calculated wavelengths and energies, and calculated orbital characteristics of the bands in the UV/Vis spectra of DAD molecules. All transitions are of $^1B \longleftarrow {}^1A$ symmetry

λ_{max}/nm (Energy/eV)			
Compound **2** (exp)[a]	Compound **1** (calc)	Compound **2** (calc)	Principal character of initial and final MOs
376 (3.30)	505 (2.45)	514 (2.41)	Aryl e_1 π/DAD N ⟶ DAD π_3 (97%, **1**; 95%, **2**)
		441 (2.81)	^{i}Pr$_3$Si σ ⟶ DAD π_3 (96%)
265 (4.68)	334 (3.71)	342 (3.62)	DAD π_2/acetylene π ⟶ DAD π_3 (65%, **1**; 50%, **2**, plus acetylene π ⟶ DAD π_3 (26%))
	330 (3.76)	340 (3.64)	DAD N lone pair/aryl e_1 ⟶ acetylene π*/DAD π_4 (59%, **1**; 67%, **2**)
	308 (4.02)	328 (3.78)	Acetylene π ⟶ DAD π_3 (83%, **1**; 65%, **2**)
		319 (3.88)	Acetylene π/^{i}Pr$_3$Si σ ⟶ acetylene π*/DAD π_4 (69%)
		304 (4.08)	^{i}Pr$_3$Si σ ⟶ acetylene π*/DAD π_4 (79%)
		293 (4.23)	^{i}Pr$_3$Si σ/DAD N lone pair/acetylene ⟶ DAD π_3
		289 (4.29)	^{i}Pr$_3$Si gs/acetylene ⟶ DAD π_3
		283 (4.38)	^{i}Pr$_3$Si σ/acetylene ⟶ DAD π_3
Compound **6** (exp)[a]	Compound **3** (calc)		
486 (2.55)	551 (2.25)		Dimethylamino N p_π/aryl e_1 π/DAD π_2 ⟶ DAD π_3 (96%)
322, sh. (3.85)	406 (3.05)		DAD N lone pair ⟶ DAD π_3 (97%)
	381 (3.25)		Dimethylamino N p_π/aryl e_1 π/DAD π_3 ⟶ DAD π_4/ acetylene π* (88%)
264 (4.69)	325 (3.81)		Dimethylamino N p_π/aryl e_1 π/DAD π_3 ⟶ aryl e_2 (71%)
	321 (3.86)		DAD π_2/acetylene π/aryl e_1 ⟶ DAD π_3 (82%)
	296 (4.19)		Acetylene π ⟶ DAD π_3 (93%)

[a] Data from reference 9.

that the most stable orientation of the aryl rings was for a C_1–N–C_4–C_5 dihedral angle of 0°. Furthermore, the total molecular bonding energy was found to be largely unaffected by increasing this dihedral angle up to *c.* 35°, and hence there is a wider range of structures which contribute to the absorption spectrum than was found for **1**. It should also be noted that the Me_2N groups were almost coplanar with the aryl rings in the optimised geometries, implying sp^2 hybridisation at the dimethylamino N atoms.

The calculated transition wavelengths for **3** are given in Table 4. As with **1**, the calculation predicts all of the bands to lie at wavelengths which are longer than is found experimentally. Our calculations agree with experiment in that they find that the longest wavelength transition in **3** is significantly shifted bathochromically in comparison with that of **1**. The computational shift of 46 nm is less than is observed experimentally, but is nevertheless quite substantial. It is pleasing to note that this shift in energy is accompanied by a change in the character of the starting orbital responsible for this transition. Thus, while the finishing orbital is once again the DAD π_3 LUMO, the starting MO (32b HOMO) is now a mixture of DAD π_2, aryl e_1 and, crucially, the p_π AO of the N atoms of the dimethylamino groups. This MO is shown in Fig. 4, from which it may be seen that the Me_2N N atom contribution is substantial. This is an important result as it makes a direct connection between the Me_2N substitution on the aryl ring and the bathochromic shift of the longest wavelength transition.

Our calculations find three absorptions in **3** which we equate with the higher energy experimental band (at 264 nm in **6**). These are calculated to have wavelengths of 325, 321 and 296 nm respectively (Table 4), of which the 321 nm transition is the most intense. The localisation properties of the MOs responsible for the 321 nm transition are broadly similar to the analogous transition in **1** (at 334 nm). The destination orbital is the mainly DAD π_3 34a LUMO. †† Unlike in **1**, however, there are two starting MOs (30b HOMO-4 and 29b HOMO-6), promotions from which make up 44% and 38% respectively of the overall $^1B \longleftarrow {}^1A$ transition. These starting MOs are a mixture of DAD π_2 and acetylene π (as for **1**), with an additional contribution from aryl e_1. Crucially, none of the MOs giving rise to the 321 nm absorption (30b, 29b and 34a) has a major contribution from the dimethylamino N atoms, and hence the energy of the transition is largely unaffected on *para* substitution of the aryl rings.

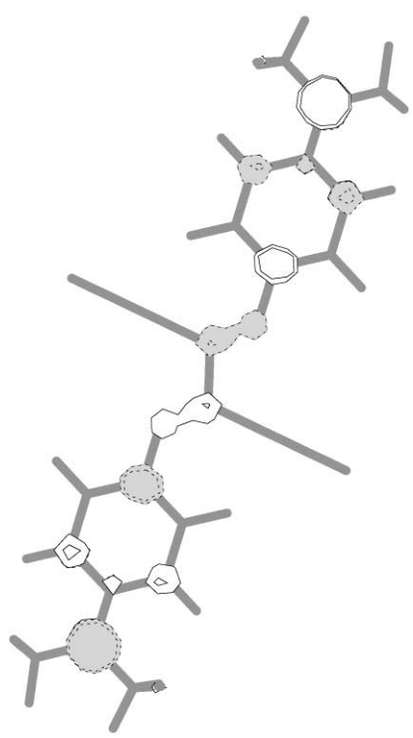

Fig. 4 Three-dimensional representation of the 32b HOMO of **3**.

Of the two other calculated transitions in **3** which we equate with the experimental band at 264 nm, the longer wavelength absorption (at 325 nm) is primarily composed of promotion of an electron from the 33a HOMO-1 to the 34b LUMO+3. The

†† This MO contains smaller contributions from C3, the aryl e_1 levels and indeed the dimethylamino N atom. However, the principal contributor is certainly the DAD π_3. Indeed, this MO is not unlike the LUMO of **1** (Fig. 3(b)).

33a orbital is a mixture of DAD π_3, aryl e_1 and dimethylamino N p_π, the latter perhaps explaining why an analogous transition is not seen in **1**. The higher energy transition, at 296 nm, is calculated to be very weak, and is the equivalent of the 308 nm transition found in **1**.

As noted above, the experimental spectrum of **6** has a 322 nm shoulder which is not seen for **2**. We equate our calculated transitions at 406 and 381 nm for **3** with this shoulder. Of the two transitions the 381 nm is the more intense, and is primarily due to promotion of an electron from the 33a HOMO-1 to the 33b LUMO+1, of mixed DAD π_4–acetylene π^* character. The discrepancy between theoretical and experimental wavelength for this transition (*c.* 60 nm) is comparable with that of the other transitions.

When comparing the spectra of **1** and **2** (Fig. 2) we arbitrarily set the calculated and experimental intensities of the longest wavelength peak to be equal. If we do the same for **3** and **6** (not shown) we find that the calculated intensity of the 321 nm peak is significantly smaller than the equivalent experimental band. Thus, as with **1** and **2**, the calculation does not exactly reproduce the relative intensity of the two peaks. However, the calculation finds that the longer wavelength peak in **3** is significantly more intense than the short wavelength peak, as is found experimentally in **6**.

B4 Comparison of the calculated and experimental electronic absorption spectra of 2. Thus far we have compared the experimental spectra of molecules with $^{i}Pr_3Si$ groups attached to the acetylene units with the computed spectra of simplified structures in which the $^{i}Pr_3Si$ groups are replaced by H atoms. The motivation for this simplification is, of course, computational feasibility; the $^{i}Pr_3Si$ substituted molecules are very large to be addressed by a full quantum mechanical approach. As described in sections B2 and B3, we believe that we can use the calculated spectra of the H substituted systems in order to interpret those obtained experimentally on the $^{i}Pr_3Si$ substituted molecules. As noted in the Introduction, however, we felt that it was important to discover if the H/ $^{i}Pr_3Si$ substitution significantly affects the simulated spectra, and hence we have calculated the electronic transition energies of **2**. These calculations proved to be extremely time consuming, even on EV68 Compaq ES40 machines.

As with **1** and **3**, we have calculated the electronic transition energies of **2** in dichloromethane solvent, assuming that the (*E*-s-*trans*-*E*) orientation prevails in solution. Calculation of the total molecular bonding energy as a function of C_1–N–C_4–C_5 dihedral angle produced results very similar to those shown in Fig. 1 for **1**, with the minimum energy conformation at just above 50°. As before, we have calculated the electronic transition energies of conformations around the minimum energy structure, and have Boltzmann-weighted these in order to construct our computational absorption spectrum. This is shown in Fig. 5, with the transition energies and assignments collected in Table 4.

Comparison of Figs. 5 and 2 and examination of Table 4 reveal that the introduction of $^{i}Pr_3Si$ groups significantly increases the complexity of the calculated absorption spectrum. Encouragingly, however, the three significant transitions found for **1** are also present in **2**. Thus the longest wavelength peak in the calculated spectrum of **2** is, as in **1**, due almost entirely to the promotion of an electron from the HOMO to the LUMO (53b ⟶ 55a). Unlike in **1**, however, our calculations find a less intense transition in **2** at 441 nm, which lies quite close to the longest wavelength peak. While the destination orbital in the associated transition is once again the 55a LUMO, the starting orbital is now the 51b HOMO-6, which is almost entirely localised on the $^{i}Pr_3Si$ fragments.

The next calculated transition comes at 342 nm, and is, in orbital terms, the closest equivalent of the 334 nm absorption found in **1**. The destination MO for the primary electron promotion (50%) responsible for this absorption is again the DAD π_3 LUMO, while the starting MO is the 49b HOMO-8. A second electron promotion also contributes significantly to this transition (26%), involving the mainly acetylenic π bonding HOMO-11 level and the LUMO. As with the longest wavelength transition, the 342 nm transition in **2** is slightly shifted bathochromically in comparison with the analogous transition in **1**.

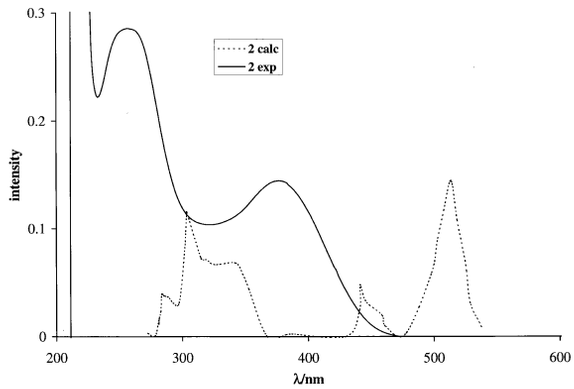

Fig. 5 The experimental (solid line) and simulated (dashed line) UV/Vis absorption spectrum of **2**. The intensity of the longest wavelength peak in the simulated spectrum has been set equal to that in the experimental spectrum.

As in **1** our calculations for **2** find a transition almost isoenergetic with that at 342 nm. This transition, at 340 nm, contains a significant amount of 54a HOMO-1 ⟶ 54b LUMO+1 character. The next calculated transition lies at 328 nm, and is the equivalent of the low intensity 308 nm transition in **1**, *i.e.* the primary MO character of this transition is the HOMO-11 acetylene π level ⟶ 55a DAD π_3 LUMO. We subsequently find a whole series of transitions in a narrow wavelength/energy range (*c.* 320–280 nm). None of these transitions was found in **1** and, in keeping with this, all of the starting MOs in the associated electron promotions contain a significant amount of σ character from the $^{i}Pr_3Si$ units.

B5 Is it necessary to include the acetylenic $^{i}Pr_3Si$ substituents in computational models? It is not completely clear from our calculations whether it is necessary to include the $^{i}Pr_3Si$ groups in order to adequately model the experimental absorption spectrum of **2**. As discussed in section B2, we can assign the experimental spectrum of **2** on the basis of calculations on the model compound **1**. Inclusion of the $^{i}Pr_3Si$ groups in the computational model produces the more complicated spectrum shown in Fig. 5, but this can also be reconciled with the experimental spectrum. Assuming that the calculated peak at 514 nm equates to the experimental one at 376 nm, the calculated 441 nm transition could quite easily be present in the experimental spectrum in the 320 nm region. Indeed, this may be the reason why there is no clear separation of the two bands in the experimental spectrum. Furthermore, we cannot exclude the possibility that the higher energy experimental peak has more than one contributing absorption.

On balance, we conclude that the present work does not conclusively prove that it is necessary to include the $^{i}Pr_3Si$ groups. Given that our ultimate aim is to rationalise and predict the UV/Vis spectra of DAD complexes of palladium, which are even more computationally demanding than the present systems, we anticipate that H (or perhaps H_3Si) substituted ligands will be used in these calculations.

Summary and conclusions

In this contribution we have reported the results of TD-DFT studies of the electronic transition energies of substituted

DADs. Given that we had little previous experience with TD-DFT methods, and that the field itself is quite new, we began by establishing a computationally tractable model chemistry. We found that the local density approximation was quite sufficient, in conjunction with dz1p basis sets (and the Klamt surface for the inclusion of solvent effects *via* the COSMO approach). The addition of gradient corrections and/or improvements in basis set quality were found to be unnecessary.

We then took this computational methodology and applied it to the geometric structures of compounds **1**, **2** and **3** (see Scheme 1 for compound definitions). Good agreement was found between the metric parameters of these systems and those determined experimentally for compounds **4** and **5**. One structural feature of **4** and **5** that was reasonably successfully reproduced by our calculations, at least for **1** and **2**, is the C_1–N–C_4–C_5 dihedral angle, which is considerably larger than 0°, *i.e.* the aryl rings are significantly rotated out of the plane of the DAD backbone. This proved to be very important when it came to calculating the electronic transition energies of **1**, **2** and **3**, as the energy and intensity of the key low energy transitions were found to be strongly dependent upon the aryl ring dihedral angle. Given that the potential energy surface for rotation of the aryl rings around the N–C_4 vector is very shallow in all cases, we concluded that electronic transitions would occur in solution from molecules with a variety of aryl ring orientations, and that the experimental spectra could not, therefore, be modelled correctly by a single molecular geometry. We attempted to take account of this in our simulated spectra by calculating the electronic transition energies and intensities for molecules with aryl ring orientations around the potential energy minimum, with subsequent weighting of the energies/transitions by a Boltzmann factor derived from the relative energies of the geometric structures.

Comparison of the simulated spectrum of **1** with the experimentally determined spectrum of **2** proved quite successful. The two experimental peaks above *c.* 200 nm were reproduced computationally, although calculation overestimates the wavelength of both peaks by *c.* 100 nm, a discrepancy typical of current TD-DFT methods. The longest wavelength peak was found to be due to promotion of an electron from the HOMO (of mixed aryl ring pπ and DAD N character) to the DAD π_3 LUMO. The higher energy absorption is assigned to a predominantly DAD π_2 (with some acetylene π) ⟶ DAD π_3 transition.

We also compared the calculated transitions of **3** with those found experimentally for **6**. These calculations also yielded some pleasing results. Experimentally, the higher energy peak in the spectra of both **2** and **6** lies at the same wavelength (265 nm), implying that the MO nature of the corresponding electronic transition is unaffected by *para* substitution of the aryl rings with dimethylamino groups. Computationally we found that the main associated electronic transition in **3** is very similar to that discussed above for **1**, and has very little Me_2N character. By contrast, the longest wavelength peak in the spectrum of **6** is significantly shifted bathochromically with respect to the analogous peak in **2**. This is nicely rationalised computationally as the HOMO in **3** has very significant Me_2N character, leading to a reduction in the HOMO–LUMO gap in comparison with **1**, and hence to a longer wavelength transition.

Our final study focused on **2**. Specifically we were keen to establish if it is necessary to include the computationally demanding $^iPr_3Si$ substituents on the acetylene groups, or if **1** can be used as a good guide to understanding the experimental spectrum of **2**. Calculations on the full **2** proved very time consuming, and produced a simulated spectrum which is of arguably poorer quality than that obtained using the much simpler **1**. The extension of the present study to DAD complexes of palladium, currently beginning in our group, will therefore focus on DAD ligands with H-substituted acetylene units.

Acknowledgements

We are grateful to University College London for a Teaching Assistantship to LEF, and to the University of London's Central Research Fund and HEFCE/EPSRC (through the Joint Research Equipment Initiative) for equipment grants.

References

1 R. Bonnet, *Chem. Soc. Rev.*, 1995, 19.
2 L. Milgrom and S. MacRobert, *Chem. Br.*, 1998(5), 45.
3 R. Bonnet, *Rev. Contemp. Pharmacother.*, 1999, **10**, 1.
4 H. Ali and J. E. van Lier, *Chem. Rev.*, 1999, **99**, 2379.
5 B. Franck and A. Nonn, *Angew. Chem.*, 1995, **107**, 1941.
6 I. Rosenthal, in *Phthalocyanines—Properties and Applications*, eds. C. C. Leznoff and A. B. P. Lever, VCH, Weinheim, 1996, vol. 4, p. 481.
7 C. M. Allen, W. M. Sharman and J. E. van Lier, *J. Porphyrins Phthalocyanines*, 2001, **5**, 161.
8 R. Faust and F. Mitzel, *J. Chem. Soc., Perkin Trans. 1*, 2000, 3746.
9 R. Faust, B. Göbelt, C. Weber, C. Krieger, M. Gross, J.-P. Gisselbrecht and C. Boudon, *Eur. J. Org. Chem.*, 1999, 205.
10 R. Faust, B. Göbelt and C. Weber, *J. Organomet. Chem.*, 1999, **578**, 186.
11 B. Göbelt, PhD Thesis, University of Heidelberg, 1999.
12 E. Runge and E. K. U. Gross, *Phys. Rev. Lett.*, 1984, **52**, 997.
13 S. J. A. van Gisbergen, J. G. Snijders and E. J. Baerends, *Comput. Phys. Commun.*, 1999, **118**, 119.
14 S. J. A. van Gisbergen, J. A. Groeneveld, A. Rosa, J. G. Snijders and E. J. Baerends, *J. Phys. Chem. A*, 1999, **103**, 6835.
15 N. N. Matsuzawa, A. Ishitani, D. A. Dixon and T. Uda, *J. Phys. Chem. A*, 2001, **105**, 4953.
16 L. Gobbi, N. Elmaci, H. P. Lüthi and F. Diederich, *Chem. Phys. Chem.*, 2001, **2**, 423.
17 ADF2000, Department of Theoretical Chemistry, Vrije Universiteit, Amsterdam, 2000.
18 E. J. Baerends, D. E. Ellis and P. Ros, *Chem. Phys.*, 1973, **2**, 41.
19 L. Versluis and T. Ziegler, *J. Chem. Phys.*, 1988, **88**, 322.
20 G. te Velde and E. J. Baerends, *J. Comp. Phys.*, 1992, **99**, 84.
21 C. Fonseca Guerra, J. G. Snijders, G. te Velde and E. J. Baerends, *Theor. Chem. Acc.*, 1998, **99**, 391.
22 S. H. Vosko, L. Wilk and M. Nusair, *Can. J. Phys.*, 1980, **58**, 1200.
23 A. Klamt, *J. Phys. Chem.*, 1995, **99**, 2224.
24 For details of both MOLDEN and ADFrom99, the reader is directed to http://www.caos.kun.nl/~schaft/molden/molden.html.
25 N. Kaltsoyannis and B. E. Bursten, *Inorg. Chem.*, 1995, **34**, 2735.
26 N. Kaltsoyannis, *J. Alloys Compd.*, 1998, **271–273**, 859.
27 A. Klamt and G. Schüürmann, *J. Chem. Soc., Perkin Trans. 2*, 1993, 799.
28 N. J. Turro, *Modern Molecular Photochemistry*, University Science Books, Mill Valley, 1st edn., 1991.